Journal of Nuclear Medicine, published on November 28, 2013 as doi:10.2967/jnumed.113.121897

In Vivo Detection of Monoaminergic Degeneration in Early Parkinson Disease by ^{18}F-9-Fluoropropyl-(+)-Dihydrotetrabenzazine PET

Shao-Cheng Lin*[1], Kun-Ju Lin*[2–4], Ing-Tsung Hsiao[4,5], Chia-Ju Hsieh[4,5], Wey-Yil Lin[1,6], Chin-Song Lu[1,6,7], Shiaw-Pyng Wey[3,4], Tzu-Chen Yen[2,3], Mei-Ping Kung[3,4,8], and Yi-Hsin Weng[1,6,7]

[1]Department of Neurology, Chang Gung Memorial Hospital, Taoyuan, Taiwan; [2]Department of Nuclear Medicine, Chang Gung Memorial Hospital, Taoyuan, Taiwan; [3]Molecular Imaging Center, Chang Gung Memorial Hospital, Taoyuan, Taiwan; [4]Department of Medical Imaging and Radiological Sciences, Chang Gung University, Taoyuan, Taiwan; [5]Healthy Aging Research Center, Chang Gung University, Taoyuan, Taiwan; [6]Neuroscience Research Center, Chang Gung Memorial Hospital, Taoyuan, Taiwan; [7]School of Medicine, Chang Gung University, Taoyuan, Taiwan; and [8]Department of Radiology, University of Pennsylvania, Philadelphia, Pennsylvania

PET with ^{18}F-9-fluoropropyl-(+)-dihydrotetrabenzazine (^{18}F-DTBZ), a novel radiotracer targeting vesicular monoamine transporter type 2 (VMAT2), has been proven as a useful imaging marker to measure dopaminergic integrity. **Methods:** The aim of this study was to evaluate the capability of ^{18}F-DTBZ PET in detecting the monoaminergic degeneration in early Parkinson disease (PD) in vivo. Seventeen age-matched healthy subjects and 30 PD patients at early stage of disease (duration of disease ≤ 5 y) with mild and unilateral motor symptoms underwent ^{18}F-DTBZ PET scans. The severity of disease, including Unified Parkinson Disease Rating Scale and modified Hoehn and Yahr Stage (mHY), were recorded at off-medication states. The standardized volumes of interest were applied to the spatial normalized image for quantification analysis. The specific uptake ratios (SURs) were calculated according to the formula (specific volumes-of-interest counts/occipital cortex counts) − 1. SUR measurements were summarized for each brain region. **Results:** The mean duration of disease in the PD group was 3.2 ± 2.1 y (range, 0.5–5 y). The mean mHY was 1.0 ± 0.1 (range, 1–1.5). The SURs of bilateral caudate, anterior putamen, posterior putamen, substantia nigra, and nucleus accumbens were significantly lower in PD patients than those of healthy subjects. The reduction of SURs was most severe in the contralateral (the brain regions that are located opposite to the symptomatic side) posterior putamen (−81%), followed by the ipsilateral posterior putamen (−67%). Receiver-operating-characteristic curve analysis showed that the SURs of the bilateral posterior putamen and contralateral anterior putamen had a sensitivity of 100% and specificity of 100% in differentiating PD patients from healthy subjects. **Conclusion:** ^{18}F-DTBZ PET was as an excellent tool for the early diagnosis of PD. The obvious decline of ^{18}F-DTBZ uptake in the ipsilateral (asymptomatic) striatum suggested that ^{18}F-DTBZ PET might serve as an in vivo biomarker to detect the monoaminergic degeneration in the premotor phase of PD.

Key Words: VMAT2; ^{18}F-DTBZ PET; Parkinson's disease

J Nucl Med 2014; 55:1–7
DOI: 10.2967/jnumed.113.121897

Parkinson disease (PD) is the second most frequent neurodegenerative disorder after Alzheimer disease in the elderly population, affecting between 0.5% and 1% of the population aged 65–69 y and increasing to 1%–3% of the population over 80 y of age (*1,2*). The 4 cardinal motor symptoms of PD include resting tremor, rigidity, bradykinesia, and postural instability. The underlying pathologic finding in PD is the progressive loss of dopaminergic neurons in the substantia nigra (SN) and other monoaminergic cell groups in the brain stem (*3*). The current diagnosis of PD is based on the clinical symptoms and a favorable response to levodopa therapy. Several proposed clinical criteria have been established (*4,5*). However, the misdiagnosis rates are as high as 20%–30% in early stages (*6,7*).

For early diagnosis and further management, practical laboratory assistance is required. Various objective measures have been suggested in the diagnosis of PD, including the olfactory function, electrophysiologic, and neuropsychologic tests (*8*). However, the most developed area in terms of providing an objective assessment is neuroimaging (*9*). Functional neuroimaging methods, such as PET and SPECT with various radioactive tracers (radioligands), can provide quantitative assessment of the dopaminergic system.

Presynaptic nigrostriatal neurons can be imaged by assessment of the activity of aromatic-amino-acid decarboxylase (AADC), dopamine transporter (DAT), and vesicular monoamine transporter 2 (VMAT2). VMAT2 is a specific presynaptic protein involved in the transport of monoamines from cytosol to storage vesicles of monoaminergic nerve terminals. VMAT2 density is linearly related to the integrity of SN dopamine neurons (*10,11*). In the early stage of PD, AADC that controls dopamine synthesis is upregulated. DAT that controls the reuptake of synaptic dopamine is downregulated (*12,13*). The VMAT2 availability is relatively less affected by this compensatory regulation (*11–13*). Therefore,

Received Feb. 28, 2013; revision accepted Jul. 16, 2013.
For correspondence or reprints contact: Yi-Hsin Weng, Department of Neurology, Chang Gung Memorial Hospital, No5, Fuxing 1st Rd., Guishan Township, Taoyuan County 333, Taiwan.
E-mail: yhweng2488@gmail.com
*Contributed equally to this work.
Published online ■■■■■■■■■■■■.

PET radioligands that target VMAT2 have been proposed to be a better biomarker for quantification of the dopamine presynaptic neurons (*12–14*). Several studies showed the suitability of ^{11}C-dihydrotetrabenazine (^{11}C-DTBZ) PET for objective quantification of nigrostriatal integrity (*15,16*). The mean striatal ^{11}C-DTBZ binding values in early, untreated PD patients were significantly decreased as compared with control subjects (*16*). However, the short half-life of ^{11}C precluded its utility for large-scale survey.

^{18}F-9-fluoropropyl-(+)-dihydrotetrabenzazine (^{18}F-DTBZ), a novel VMAT2 ligand, has high affinity and specificity of binding to VMAT2 (*17*). Animal studies conclude that ^{18}F-DTBZ is a sensitive and selective tracer for VMAT2 binding sites, and it may be useful for in vivo evaluation of diseases relating to changes of monoamine neuronal integrity (*10,18*). Our previous study showed that ^{18}F-DTBZ PET was safe, with appropriate biodistribution and radiation dosimetry for imaging VMAT2 sites in humans (*19*). Therefore, we conducted this study to evaluate the capability of ^{18}F-DTBZ PET imaging in detecting the monoaminergic degeneration in early PD in vivo and to test the sensitivity and specificity of ^{18}F-DTBZ PET in differentiating early PD from normal aging.

MATERIALS AND METHODS

Subjects

The study protocol was approved by the Institutional Review Board of the Chang Gung Memorial Hospital and the Governmental Department of Health. Written informed consent was obtained before all procedures for each participant. Healthy controls (HCs) were recruited by advertisement in the community. Patients who fulfilled the U.K. Parkinson Disease Society Brain Bank Clinical Diagnostic Criteria were recruited from movement disorder clinics of Chang Gung Memorial Hospital. The PD patients should have unilateral symptoms (i.e., the modified Hoehn and Yahr stage [mHY] should be $\leq$ 1.5). The duration of disease should be less than or equal to 5 y. Forty-seven subjects, including 30 PD patients aged 53.2 $\pm$ 10.1 y (mean $\pm$ SD; range, 30–71 y) and 17 HCs aged 56.8 $\pm$ 4.0 y (range, 51–64 y), were enrolled. All subjects received neurologic examination and the assessment of Unified Parkinson Disease Rating Scale and mHY by 2 experts in movement disorders. The neurologic examination and PET scanning were performed at the drug-off state (subjects should not take any antiparkinsonian medication at least 12 h before the tests). To evaluate the severity of depression, anxiety, and cognitive impairment in PD patients, the Hamilton Depression Rating scale (HAM-D), Hamilton Anxiety Rating scale (HAM-A), Mini-Mental State Examination (MMSE), and Montreal Cognitive Assessment (MoCA) were assessed at the drug-on state.

Data Acquisition

^{18}F-DTBZ was prepared and synthesized at the cyclotron facility of Chang Gung Memorial Hospital as described previously (*10,19*). All subjects were studied in a Biograph mCT PET/CT System (Siemens Medical Solutions) with a 3-dimensional (3D) acquisition mode. All subjects underwent MR imaging for screening of other diseases, obtaining structural information, the purpose of generating volumes of interest (VOIs), and performing spatial normalization with PET images. Subjects were imaged on a 3T Siemens Magnetom TIM Trio scanner (Siemens Medical Solutions).

After injection of 386 $\pm$ 11 MBq of ^{18}F-DTBZ, a single 10-min PET scan was acquired 90 min after injection in a 3D model (*20*). PET images were then reconstructed using a 3D ordered-subset expectation maximization algorithm (4 iterations, 24 subsets; gaussian filter, 2 mm; zoom, 3) with CT-based attenuation correction and also scatter and random correction as provided by the manufacturer. The images were reconstructed with a matrix size of $400 \times 400 \times 148$ and a voxel size of $0.68 \times 0.68 \times 1.5$ mm.

Image Analysis

All image data were processed and analyzed using PMOD image analysis software (version 3.3; PMOD Technologies Ltd.). Each PET image was coregistered to the corresponding MR image, and the individual MR image was spatially normalized to the Montreal Neurologic Institute (MNI) MR imaging template (*21*). The spatial normalization parameters were then applied to PET images to form a final, spatially normalized PET image in the MNI domain. VOIs were defined on the automated anatomic labeling brain template in the PMOD image analysis software with some modification (*22*). VOIs for subregions were customized using a universal VOI template (*21*). For all subjects, a binary gray matter mask was created by taking the nonzero pixels from an averaged gray matter probability map generated from the segmentation of the spatially normalized MR images. To reduce the partial-volume effect as much as possible, the automated anatomic labeling atlas was then multiplied by the averaged gray matter mask to generate a custom gray matter atlas for all subjects (*23*). To explore the nigrostriatal degeneration (the motor part), VOIs of the bilateral caudate nuclei (Cau), anterior/posterior putamen (APu/PPu), and SN were selected for further analysis. To analyze the mesolimbic and serotonergic dysfunction (the nonmotor part), VOIs of the nucleus accumbens (NAc), raphe nucleus (RN), amygdala (AMG), hippocampus (HPC), and dorsolateral prefrontal cortex (DLPFC) were selected. The occipital cortex was applied as the reference region for computing binding ratio for each VOI. The standardized uptake value ratios (SUVRs) of targeted VOIs to reference region were determined for each subject, and the specific uptake ratio (SUR = SUVR – 1.0) (*24*) in each VOI was finally calculated for further analysis. In the PD group, we defined the contralateral striatum as the striatum that was located opposite to the symptomatic limbs, and the contralateral striatum was evaluated separately from the ipsilateral striatum. According to our previous studies, the uptake of ^{18}F-DTBZ was symmetric in the healthy subjects (*19,20*). For further statistical analysis, the contralateral striatum was defined as the right striatum, and the ipsilateral striatum was defined as the left striatum in the control group. For an expression of the asymmetry of VMAT2 density in the PD group, we calculated the asymmetric index (ASI) as follows: 100% $\times$ (contralateral $-$ ipsilateral)/([contralateral + ipsilateral]/2).

Voxelwise Analysis

Voxelwise analysis was performed by SPM5 (Wellcome Department of Cognitive Neurology, Institute of Neurology) in Matlab2010a (The MathWorks Inc.). In the PD patients, the ipsilateral striatum was flipped to the right side for future statistical parametric mapping (SPM) analysis. Spatially normalized SUR images of ^{18}F-DTBZ were smoothed using an isotropic gaussian kernel of 8 mm in full width at half maximum. The voxelwise 2-sample *t* test for group comparison between HC and each PD group was computed in ^{18}F-DTBZ SUR images. SPM t-maps were examined using a threshold of *P* less than 0.05 with false discovery rate correction and an extent threshold of 100 voxels.

Statistical Analysis

The regional SUR of the ^{18}F-DTBZ PET images and clinical data were statistically compared using the nonparametric Mann–Whitney test for group comparison between HCs and PD. The receiver-operative-characteristic (ROC) curves (SPSS 17.0 software; SPSS Inc.) were generated to compare the diagnostic accuracy of each SUR in differentiating PD from HCs, based on the areas under the ROC curves. A *P* value of 0.05 was defined as the threshold of statistical significance

jnm121897-pm ■ 11/27/13

TABLE 1
Clinical and Demographic Data of Subjects

Group	Age (y)	Sex (M:F)	Age of onset	Duration of disease	UPDRS-III	UPDRS total	mHY
HC (n = 17)	56.8 ± 4.0 (51–64)	6:11	—	—	0	0	0
PD (n = 30)	53.2 ± 10.1 (30–71)	20:10	50.8 ± 9.9 (29–69)	3.2 ± 2.1 (0.5–5)	7.3 ± 4.7 (2–19)	12.1 ± 7.1 (2–28)	1.0 ± 0.1 (1–1.5)

Data are mean ± SD, with ranges in parentheses.
UPDRS-III = motor score of UPDRS; UPDRS = Unified Parkinson Disease Rating Scale.

in each test after multiple-comparison post hoc test correction was applied.

RESULTS

[**Table 1**] Table 1 summarizes the demographic data. There was no difference between groups in the age at PET scan. The male-to-female ratios were not equal in the PD and HC groups. However, the SURs of ^{18}F-DTBZ in male and female subjects were similar in both PD and HC groups (Supplemental Fig. 1; supplemental materials are available at http://jnm.snmjournals.org). Thirty patients had motor symptoms at the right limbs, whereas 17 presented with left parkinsonian symptoms. All patients were at the early stage of PD (the duration of disease was 0.5–5 y), with only mild and unilateral motor symptoms (the off-medication state mHY: stage 1, n = 28; stage 1.5, n = 2). The PD patients had no obvious dementia: the mean score of MMSE and MoCA was 29.0 ± 1.2 (range, 26–30) and 27.3 ± 1.9 (range, 24–30), respectively. The mean score of HAM-D and HAM-A was 4.1 ± 4.3 (range, 1–17) and 4.3 ± 1.3 (range, 0–16), respectively.

[**Fig. 1**] Figure 1 shows the ^{18}F-DTBZ PET images in a PD patient (Fig. 1B) and an age-matched healthy subject (Fig. 1A). The uptake of ^{18}F-DTBZ was symmetric and clearly visible in the SN, RN, NAc, AMG, and striatum in the healthy subject. In the PD patient, the VMAT2 density was obviously decreased in the bilateral caudate, putamen, contralateral SN, and NAc by visual assessment. The uptake of ^{18}F-DTBZ was asymmetric and gradually decreased by a rostral-to-caudal gradient, with more prominent reduction in contralateral PPu in the PD patient.

[**Table 2**] Table 2 summarizes the regional SURs of ^{18}F-DTBZ in PD patients and HCs. The SURs of bilateral Cau, APu, PPu, SN, and NAc were significantly lower in the PD group than in the HC group (all $P < 0.005$). As compared with HCs, the SURs of RN, bilateral HPC, and AMG had no significant reduction in PD patients. The reduction of ^{18}F-DTBZ uptake was greatest in the contralateral PPu (−81%), followed by ipsilateral PPu (−67%), contralateral APu (−59%), contralateral NAc (−47%), and ipsilateral APu (−45%). In HCs, the SURs had no difference between right and left hemispheres. The uptake of ^{18}F-DTBZ in all subregions was symmetric in HCs, whereas the decline of VMAT2 activity was obviously asymmetric in the PD group. The asymmetry of VMAT2 density was most pronounced in PPu, with the ASI of −53.9%, followed by APu (−31.9%), NAc (−19.7%), Cau (−19.3%), and SN (−18.2%), as shown in Figure 2.

[**Fig. 2**]

[**Fig. 3**] Figure 3 shows the SURs of ^{18}F-DTBZ in the subregions in the PD and HC groups. The reduction of VMAT2 activity was greatest in the bilateral PPu. The SURs of the contralateral and ipsilateral PPu in PD patients could be clearly separated from HCs without any overlap between the 2 groups, as shown in Figure 3. ROC curve analysis showed that the SURs of PPu and contralateral APu had a sensitivity of 100% and specificity of 100% in differentiating early PD from normal aging (Figs. 4A–C). The area under the

[**Fig. 4**]

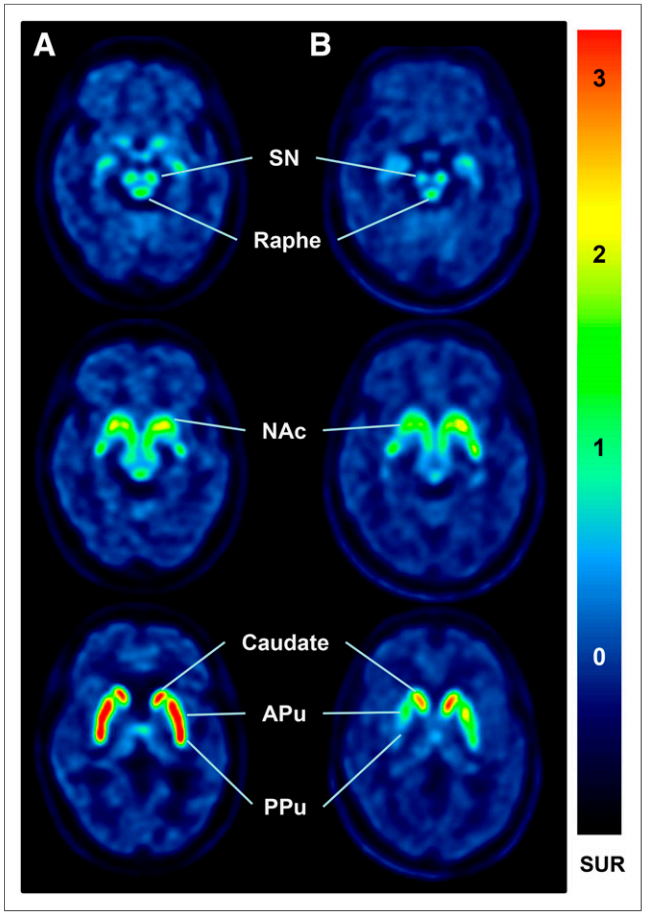

RGB

FIGURE 1. Representative ^{18}F-DTBZ PET images in healthy subject and PD patient. A 50-y-old female healthy subject (A) and a 48-y-old female patient with 3-y history of tremor and bradykinesia at left extremities (mHY stage I) (B). In PD patient, uptake of ^{18}F-DTBZ was markedly decreased in bilateral striatum with rostral-to-caudal gradient (predominantly at PPu). The VMAT2 activity was also decreased in contralateral SN and NAc by visual assessment. Regional SURs in healthy subject and PD patient were RN, 1.31 and 1.22; C-Cau, 3.11 and 1.64; C-APu, 3.21 and 1.58; C-PPu, 3.15 and 0.75; C-SN, 1.34 and 0.81; C-NAc, 1.23 and 0.85; I-Cau, 3.24 and 2.27; I-APu, 3.3 and 1.98, I-PPu, 3.49 and 1.76; I-SN, 1.47 and 0.96; and I-NAc, 1.49 and 1.61, respectively. C = contralateral; I = ipsilateral.

jnm121897-pm ■ 11/27/13

TABLE 2
SURs of ^{18}F-DTBZin Defined Regions of PD Patients and HCs

Region	HC (n = 17)	PD (n = 30)	P	Percentage of decline
RN	1.2 ± 0.3	1.1 ± 0.2	0.5208	—
C-Cau	2.5 ± 0.4	1.6 ± 0.5	<0.0001	36%
C-APu	2.9 ± 0.5	1.2 ± 0.4	<0.0001	59%
C-PPu	2.8 ± 0.4	0.5 ± 0.2	<0.0001	81%
C-SN	1.1 ± 0.2	0.7 ± 0.2	<0.0001	39%
C-HPC	0.3 ± 0.1	0.3 ± 0.1	0.5724	—
C-AMG	0.5 ± 0.1	0.5 ± 0.2	0.2362	—
C-NAc	1.6 ± 0.7	0.8 ± 0.3	<0.0001	47%
I-Cau	2.4 ± 0.5	1.9 ± 0.5	0.0011	20%
I-APu	2.9 ± 0.5	1.6 ± 0.5	<0.0001	45%
I-PPu	2.8 ± 0.5	0.9 ± 0.4	<0.0001	67%
I-SN	1.2 ± 0.3	0.8 ± 0.3	0.0001	31%
I-HPC	0.3 ± 0.1	0.3 ± 0.1	0.8248	—
I-AMG	0.5 ± 0.1	0.5 ± 0.2	0.3191	—
I-NAc	1.6 ± 0.5	1.0 ± 0.5	0.0008	35%
C-DLPFC	1.1 ± 0.1	0.9 ± 0.1	0.0119	18%

C (contralateral) = brain regions located opposite to symptomatic limbs (PD group) or right brain (HC group); I (ipsilateral) = brain regions located at side with clinical symptoms or left brain (HC group); DLPFC = dorsolateral prefrontal cortex.

ROC curve for the regional SURs was highest in bilateral PPu and contralateral APu (1.00), followed by ipsilateral APu (0.98) and contralateral Cau (0.92), as shown in Figure 4D.

As compared with the HC group, voxelwise analysis also showed that the uptake of ^{18}F-DTBZ was significantly decreased in the bilateral SN, NAc, and striatum. The VMAT2 density in the contralateral DLPFC was also significantly lower in the [Fig. 5] PD group than in the HCs (Fig. 5). The spillover effect mainly from the smoothing preprocessing caused some decreased uptake signal in white matter and also in the surrounding areas of striatum.

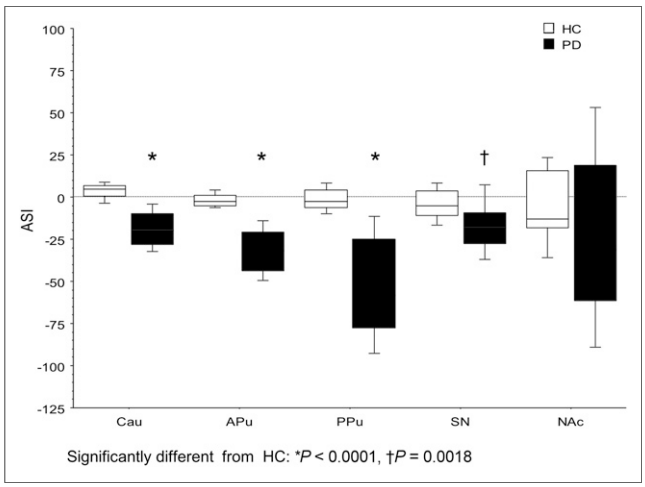

FIGURE 2. ASI of ^{18}F-DTBZ SURs in striatum, SN, and NAc. Compared with HCs, PD patients had significantly asymmetric uptake of ^{18}F-DTBZ in Cau, APu, and PPu (all $P < 0.0001$) and SN ($P = 0.0018$).

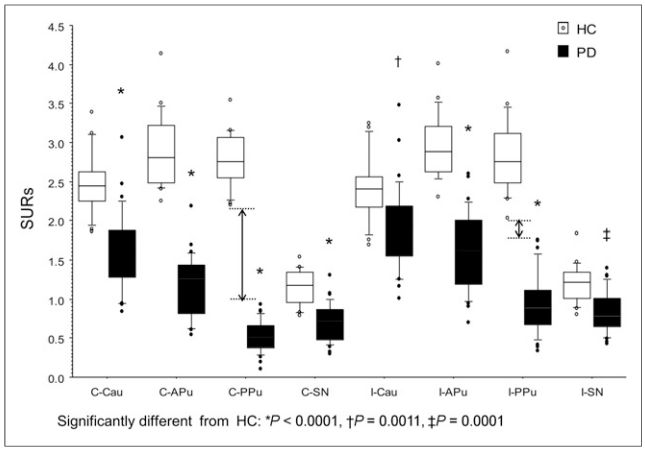

FIGURE 3. Regional SURs of^{18}F-DTBZ from VOI analysis in early PD patients and HCs. SURs of bilateral Cau, APu, PPu, and SN were significantly lower in early PD patients than in HCs. Dotted lines and 2-head arrow lines denote that SURs of contralateral and ipsilateral PPu were good markers to clearly separate the 2 groups without any overlap.

DISSCUSSION

Accurate diagnosis in patients with parkinsonism as early as possible is critical for the management of PD, including the avoidance of unnecessary medical therapies and examinations, the reduction of costs and adverse effects, and the early intervention of neuromodulation therapies. To date, early diagnosis of PD is still an unmet need. The diagnosis of PD is based on the identification of clinical characteristics, such as the cardinal motor signs, asymmetric onset, favorable levodopa responsiveness, other motor features, and nonmotor symptoms (*5*). However, these clinical features are not specific to PD. The diagnostic accuracy in the early stage of disease is still unsatisfied using clinical diagnostic criteria. Although experts in the field of movement disorders can make more accurate diagnosis of PD with the sensitivity of 91% (*24*), the initial diagnostic accuracy of PD made by general neurologists was only 65%–76% (*6,7*). By modifying the criteria, the specificity of diagnosis was increased (93%), but the sensitivity was only 68% (*7*). Thus, an increase in positive predictive value was associated with a decrease in sensitivity. The time to reach the correct clinical diagnosis could be up to 18 y (*6*).

The pathologic hallmark of PD is the degeneration of monoaminergic system, particularly in dopaminergic neurons and axons of the nigrostriatal pathway. Therefore, PET and SPECT imaging with ligands targeting the dopaminergic system provides great help in the early diagnosis of PD (*25–28*). The current available PET and SPECT imaging for the evaluation of the function of dopamine terminals in vivo include ^{18}F-DOPA PET (AADC activity), tropane-based PET (^{11}C-RTI-32, ^{18}F-2β-carbomethoxy-3β-(4-fluoro)tropane [^{18}F-CFT]) and SPECT (^{123}I-(−)-2bcarbomethoxy-3b-(4-iodophenyl) tropane [^{123}I-β-CIT], ^{123}I-2β-carbomethoxy-3β-(4-iodophenyl)-*N*-(3-fluoropropyl)nortropane [^{123}I-FP-CIT], ^{123}I-altropane, [2-[[2-[[[3-(4-chlorophenyl)-8-methyl-8-azabicyclo[3,2,1]oct-2-yl]methyl](2-mercaptoethyl)amino]ethyl]amino]ethanethiolato(3-)-N2,N2,S2,S2]oxo-[1R-(exoexo)]-^{99m}Tc-technetium [^{99m}Tc-TRODAT-1]) (DAT activity), and ^{11}C-DTBZ PET (VMAT2 activity) (*25*). ^{18}F-DOPA PET has been used for many years for the evaluation of nigral dopaminergic neurons in PD and other parkinsonian disorders (*25–27*). Nevertheless, the compensatory upregulation of AADC activity in the early stage of PD resulted in a lower sensitivity of ^{18}F-DOPA

jnm121897-pm ■ 11/27/13

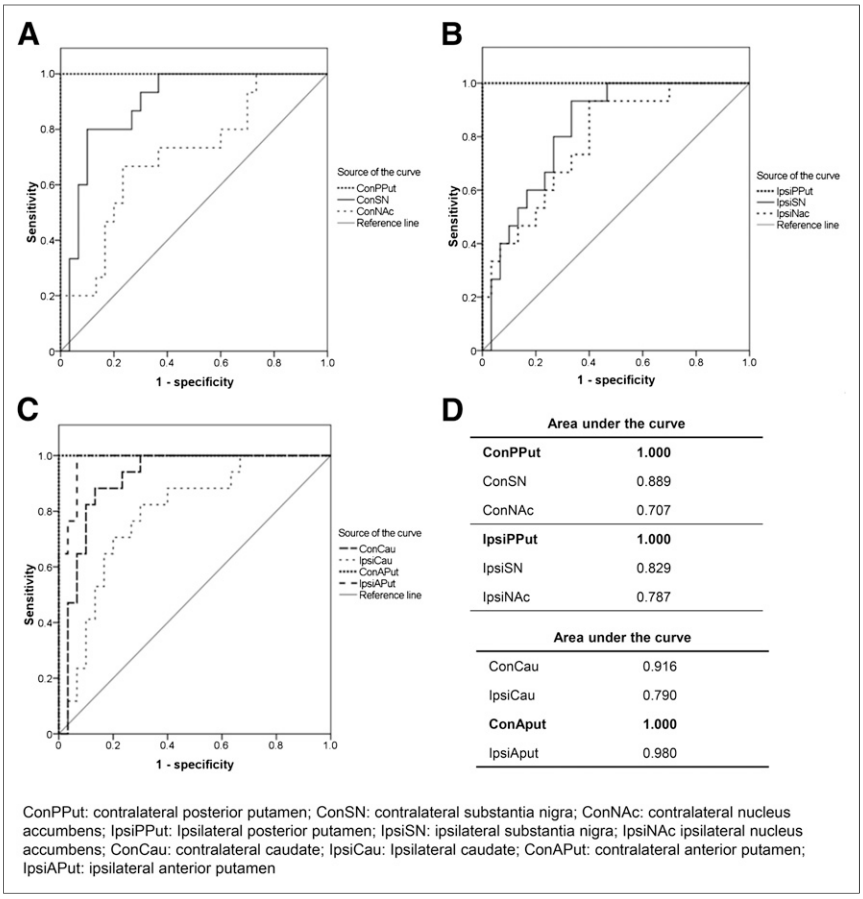

FIGURE 4. Sensitivity and specificity of ROC curve analysis of regional SURs in differentiating early PD from HC. (A) Contralateral PPu, SN, and NAc. (B) Ipsilateral PPu, SN, and NAc. (C) Contralateral and ipsilateral Cau and APu. (D) Area under curve for regional SURs. SURs of contralateral PPu (A), ipsilateral PPu (B), and contralateral APu (C) had sensitivity of 100% and specificity of 100% to distinguish early PD from HC.

PET in detecting early nigrostriatal degeneration than those of DAT and VMAT2 imaging (*12,28*). SPECT imaging with ligands targeting DAT, the most widely used imaging technique, can discriminate PD patients from healthy individuals with high sensitivity and specificity (*25,29*). However, the DAT availability is downregulated in the early stage of the disease (*12,13*). The activity of DAT may be altered by chronic drug administration (*28,30*). The low resolution of SPECT imaging also limited the utility. Although the VMAT2 availability could be transiently affected by changes in vesicular dopamine concentration (*31*), VMAT2 binding is thought to be less affected by compensation than ^{18}F-DOPA and DAT binding (*28,30*). Furthermore, a quantitative autoradiography study in normal aged human brains showed that the density of VMAT2 was significantly higher than that of DAT in both striatal and extrastriatal regions (*32*). Therefore, VMAT2 binding may provide a reliable estimate of monoaminergic nerve terminal density in humans. VMAT2 PET imaging can serve as a promising tool for the diagnosis of PD (*13,28*).

^{11}C-DTBZ PET had been proposed to be a good tool in distinguishing early, untreated PD from healthy subjects (*16*). However, the short half-life of ^{11}C (20 min) greatly limited its utility. ^{18}F has a relatively long half-life (110 min) and improves the availability for imaging VMAT2 in clinical settings. A small study of ^{18}F-DTBZ PET in 17 mild to moderate PD patients and 6 healthy subjects showed that the binding potential of ^{18}F-DTBZ was significantly decreased in the striatum and midbrain in PD patients, compared with those of HCs (*33*). In the current study, we found that the SURs of the bilateral PPu and contralateral APu had a sensitivity of 100% and specificity of 100% in differentiating PD in the early stage of disease (disease duration $\leq$ 5 y) from normal aging. The result suggested that ^{18}F-DTBZ PET imaging was a promising tool for the differential diagnosis of PD and normal aging and perhaps for the differentiation of PD from other movement disorders without presynaptic dopaminergic depletion, such as essential tremor and DOPA-responsive dystonia.

The clinical lateralization (the side that symptoms starts is always the dominantly affected side through the whole course of disease) is a clinical hallmark of PD, whereas motor symptoms in other akinetic-rigid syndromes, such as multiple system atrophy and progressive supranuclear palsy, are relatively symmetric. We found that the SURs of ^{18}F-DTBZ showed obvious asymmetry in the striatum and SN that could represent the clinical lateralization in PD. The ASI might serve as a useful index in distinguishing PD from other parkinsonism (*34,35*).

The pathology of PD is characterized by apoptosis of dopaminergic neurons in the SN particularly affecting the ventral tier of pars compacta (A9 area), which axons project to dorsal striatum (nigrostriatal pathway) (*36*). The mesolimbic system that axons project from the ventral tegmentum area (A10 area) via the NAc (ventral striatum) to the limbic system is relatively less involved. In the PD group, the decline of VMAT2 density was most severe in the PPu and APu and less affected in the NAc and caudate head as shown in Figure 1 and Table 2. Our study suggested that in vivo ^{18}F-DTBZ PET imaging could represent the uneven pattern of dopaminergic loss (caudal $>$ rostral, dorsal $>$ ventral) in PD that was confirmed by pathologic studies (*37*).

There is increased evidence suggesting that PD may start outside the SN (*3,36*). Several nonmotor symptoms, such as olfactory dysfunction, rapid eye movement sleep behavior disorder (RBD), constipation, and depression can precede the classic motor features of PD by years and even decades (*38*). The period can be referred to as the premotor phase of the disease. During the premotor phase, the neurodegeneration has started, but motor signs permitting classical diagnosis are not documented. In the current study, the uptake of ^{18}F-DTBZ in ipsilateral (the asymptomatic side) striatum and SN were also significantly decreased. ^{18}F-DTBZ PET could detect dopaminergic degeneration before motor symptoms started. We suggested that ^{18}F-DTBZ PET might be applied to the premotor (preclinical) diagnosis of PD and to the screening of at-risk populations of PD. However, this point should be verified by further studies.

The main function of the nigrostriatal system is motor control. It is not surprising that the striatal ^{18}F-DTBZ binding could

jnm121897-pm ■ 11/27/13

RGB

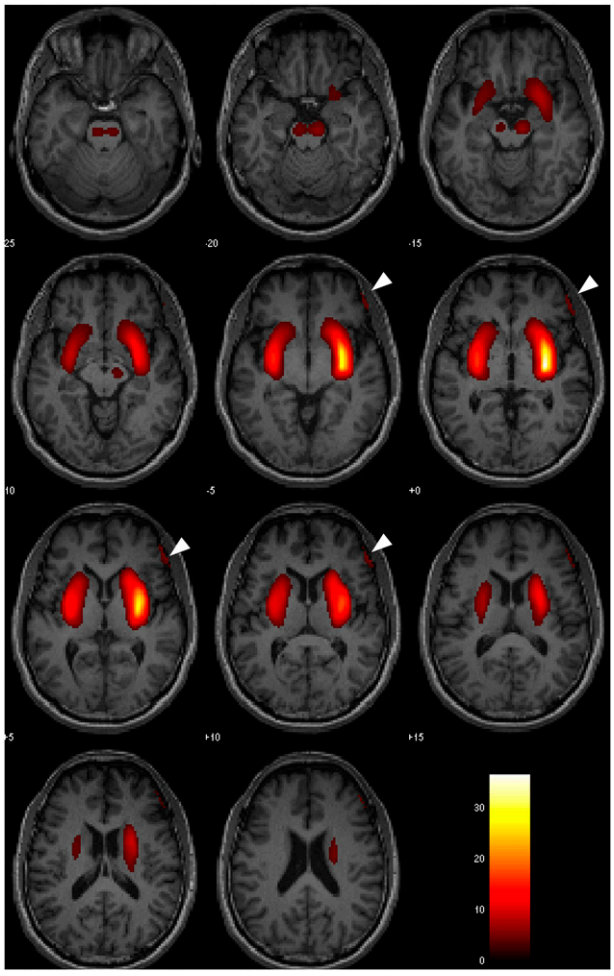

FIGURE 5. SPM analysis shows areas of reduction in ^{18}F-DTBZ SURs in PD patients, compared with HCs. As compared with HC group, ^{18}F-DTBZ uptake of bilateral SN, ventral and dorsal striatum, and dorsolateral prefrontal cortex (as indicated by arrowhead) was significantly decreased in PD group. In PD group, SURs of ^{18}F-DTBZ in contralateral regions were flipped to right side. Color bar represents t values. *P* value less than 0.05 with false discovery rate correction, extent voxel = 100.

correlate with the motor disability of PD patients (*16,33*). Because all PD subjects recruited for this study were at the similar stage of disease, we could not find any correlation between regional SURs of ^{18}F-DTBZ and all motor scores, including rigidity, bradykinesia, and tremor subscores (unpresented data). Further longitudinal study is required to evaluate the capability of ^{18}F-DTBZ PET in monitoring the severity and progression of motor and nonmotor symptoms in PD.

Nonmotor symptoms, including cognitive impairment and affective disorders, are common features in PD and have been shown to be a major determinant of quality of life of PD patients and their caregivers (*39,40*). The mesolimbic pathway arises from the ventral tegmentum area and projects to the NAc and limbic system (AMG, HPC, inferior frontal cortex, and anterior cingulate gyrus). Dopamine depletion in PD could cause the dysfunction of the mesolimbic system and frontostriatal networks and subsequently involved the cognition, emotion, motivation, and behaviors (*39,41*). In PD with dementia, ^{18}F-DOPA uptake was significantly declined in the anterior cingulate areas, NAc, and right caudate nucleus, compared with those of PD without dementia (*42*). The severity of depression, anxiety, and apathy was correlated with the activity of DAT in the limbic system (*43*). The DLPFC loop, which connected with the prefrontal area to the dorsal caudate and ventral anterior thalamus, mediates executive functions. Dopamine plays a particularly important role in the DLPFC. Impaired executive functions, apathy, and impulsivity that are common nonmotor symptoms in PD are hallmarks of DFPLC circuit dysfunction. In PD, serotonergic cells in the RN are also involved that may contribute to the development of depression (*3*). To measure the monoaminergic integrity in extrastriatal regions in vivo is important for the management of the nonmotor symptoms in PD. An in vitro autoradiography study in aged human brain showed that the density of theVMAT2 was much higher than that of DAT in extrastriatal regions (*32*). It indicated that VMAT2 imaging was superior to DAT imaging for the detection of monoaminergic degeneration in the extrastriatal regions. Therefore, to evaluate the relationship between theVMAT2 activity in the limbic system and the severity of nonmotor symptoms (HAM-D, HAM-A, MMSE, and MoCA), we further analyzed the uptake of ^{18}F-DTBZ in the NAc, HPC, AMG, RN, and DFPLC. Because all recruited PD subjects did not have dementia or obvious affective disorders, we could not find any correlation between regional SURs of ^{18}F-DTBZ and nonmotor scores. However, the VMAT2 density in the bilateral NAc and the contralateral DLPFC was significantly decreased in PD patients as compared with HCs (Table 2, Fig. 5). These findings were compatible with the reports of other functional imaging studies that demonstrated a significantly functional disruption of frontostriatal circuits in early and nondementic PD (*44,45*). Our results suggested the usefulness of ^{18}F-DTBZ PET in measuring the distribution of VMAT2 density in the mesolimbic system. However, further inference could not be drawn from current findings. The utility of ^{18}F-DTBZ PET imaging in the nonmotor symptoms of PD should be carefully validated by further studies.

There are 2 major disadvantages of ^{18}F-DTBZ PET imaging. First, like other PET examinations, is the need of a cyclotron to produce radioligands. This requirement will increase the cost and limit the utility of the clinical practice. Second, as mentioned before, the VMAT2 availability could be transiently altered by exogenous dopamine (levodopa treatment) in the advanced stage of PD (*31*). Although the effects of levodopa or dopamine agonist therapy in VMAT2 availability is not clear in the early stage of PD, all PET images were scanned at the medication-off state in this study. Nevertheless, the need of medication withdrawn may increase the suffering of patients and the complications. This issue of pharmacologic effects and test–retest reliability should be further studied.

CONCLUSION

Our study suggested that ^{18}F-DTBZ PET was an excellent tool in differentiating PD from normal aging in the early stage of disease. The notable decline of ^{18}F-DTBZ uptake in the ipsilateral striatum suggested that ^{18}F-DTBZ PET might serve as an in vivo biomarker to detect the monoaminergic degeneration in the premotor phase of PD.

DISCLOSURE

The costs of publication of this article were defrayed in part by the payment of page charges. Therefore, and solely to indicate this

jnm121897-pm ■ 11/27/13

fact, this article is hereby marked "advertisement" in accordance with 18 USC section 1734. This study was carried out with financial support from the National Science Council, Taiwan (grant NSC-98-2314-B-182-034-MY2 and 99-2314-B-182A-067-MY2, 100-2314-B-182-038, 100-2314-B-182A-092-MY3, 101-2314-B-182-061-MY2), and grants from Research Fund of Chang Gung Memorial Hospital (CMRPD1A0312, CMRPG390912, CMRPG390913). No other potential conflict of interest relevant to this article was reported.

ACKNOWLEDGMENT

We thank Avid Radiopharmaceuticals (Philadelphia, PA) for providing the precursor for the preparation of ^{18}F-DTBZ.

REFERENCES

1. de Lau LM, Breteler MM. Epidemiology of Parkinson's disease. *Lancet Neurol.* 2006;5:525–535.
2. Dorsey ER, Constantinescu R, Thompson JP, et al. Projected number of people with Parkinson disease in the most populous nations, 2005 through 2030. *Neurology.* 2007;68:384–386.
3. Braak H, Ghebremedhin E, Rub U, Bratzke H, Del Tredici K. Stages in the development of Parkinson's disease-related pathology. *Cell Tissue Res.* 2004;318:121–134.
4. Calne DB, Snow BJ, Lee C. Criteria for diagnosing Parkinson's disease. *Ann Neurol.* 1992;32:S125–S127.
5. Gelb DJ, Oliver E, Gilman S. Diagnostic criteria for Parkinson's disease. *Arch Neurol.* 1999;56:33–39.
6. Rajput AH, Rozdilsky B, Rajput A. Accuracy of clinical diagnosis in parkinsonism: a prospective study. *Can J Neurol Sci.* 1991;18:275–278.
7. Hughes AJ, Daniel SE, Kilford L, et al. Accuracy of clinical diagnosis of idiopathic Parkinson's disease: a clinico-pathological study of 100 cases. *J Neurol Neurosurg Psychiatry.* 1992;55:181–184.
8. Kashmere J, Camicioli R, Martin W. Parkinsonian syndromes and differential diagnosis. *Curr Opin Neurol.* 2002;15:461–466.
9. Brooks DJ. Assessment of Parkinson's disease by imaging. *Parkinsonism Relat Disord.* 2007;13:S268–S275.
10. Tsao HH, Lin KJ, Juang JH, et al. Binding characteristics of 9-fluoropropyl-(+)-dihydrotetrabenzazine (AV-133) to the vesicular monoamine transporter type 2 in rats. *Nucl Med Biol.* 2010;37:413–419.
11. Kilbourn MR. In vivo radiotracers for vesicular neurotransmitter transporters. *Nucl Med Biol.* 1997;24:615–619.
12. Lee CS, Samii A, Sossi V, et al. In vivo positron emission tomographic evidence for compensatory changes in presynaptic dopaminergic nerve terminals in Parkinson's disease. *Ann Neurol.* 2000;47:493–503.
13. Nandhagopal R, Kuramoto L, Schulzer M, et al. Longitudinal evolution of compensatory changes in striatal dopamine processing in Parkinson's disease. *Brain.* 2011;134:3290–3298.
14. Frey KA, Koeppe RA, Kilbourn MR, et al. Presynaptic monoaminergic vesicles in Parkinson's disease and normal aging. *Ann Neurol.* 1996;40:873–884.
15. Koeppe RA, Frey KA, Vander Borght TM, et al. Kinetic evaluation of [^{11}C] dihydrotetrabenazine by dynamic PET: measurement of vesicular monoamine transporter. *J Cereb Blood Flow Metab.* 1996;16:1288–1299.
16. Martin WR, Wieler M, Stoessl AJ, et al. Dihydrotetrabenazine positron emission tomography imaging in early, untreated Parkinson's disease. *Ann Neurol.* 2008;63:388–394.
17. Kung MP, Hou C, Goswami R, et al. Characterization of optically resolved 9-fluoropropyl-dihydrotetrabenazine as a potential PET imaging agent targeting vesicular monoamine transporters. *Nucl Med Biol.* 2007;34:239–246.
18. Goswami R, Ponde DE, Kung MP, et al. Fluoroalkyl derivatives of dihydrotetrabenazine as positron emission tomography imaging agents targeting vesicular monoamine transporters. *Nucl Med Biol.* 2006;33:685–694.
19. Lin KJ, Weng YH, Wey SP, et al. Whole-body biodistribution and radiation dosimetry of ^{18}F-FP-(1)-DTBZ (^{18}F-AV-133): a novel vesicular monoamine transporter 2 imaging agent. *J Nucl Med.* 2010;51:1480–1485.
20. Lin KJ, Lin WY, Hsieh CJ, et al. Optimal scanning time window for ^{18}F-FP-(+)-DTBZ (^{18}F-AV-133) summed uptake measurements. *Nucl Med Biol.* 2011;38:1149–1155.
21. Mazziotta JC, Toga AW, Evans A, Fox P, Lancaster J. A probabilistic atlas of the human brain: theory and rationale for its development. The International Consortium for Brain Mapping (ICBM). *Neuroimage.* 1995;2:89–101.
22. Tzourio-Mazoyer N, Landeau B, Papathanassiou D, et al. Automated anatomical labeling of activations in SPM using a macroscopic anatomical parcellation of the MNI MRI single-subject brain. *Neuroimage.* 2002;15:273–289.
23. Huang KL, Lin KJ, Hsiao IT, et al. Regional amyloid deposition in amnestic mild cognitive impairment and Alzheimer's disease evaluated by [^{18}F]AV-45 positron emission tomography in Chinese population. *PLoS ONE.* 2013;8:e58974.
24. Hughes AJ, Daniel SE, Ben-Shlomo Y, Lees AJ. The accuracy of diagnosis of parkinsonian syndromes in a specialist movement disorder service. *Brain.* 2002;125:861–870.
25. Cummings JL, Henchcliffe C, Schaier S, Simuni T, Waxman A, Kemp P. The role of dopaminergic imaging in patients with symptoms of dopaminergic system neurodegeneration. *Brain.* 2011;134:3146–3166.
26. Shen LH, Liao MH, Tseng YC. Recent advances in imaging of dopaminergic neurons for evaluation of neuropsychiatric disorders. *J Biomed Biotechnol.* 2012;2012:259–349.
27. Sioka C, Fotopoulos A, Kyritsis AP. Recent advances in PET imaging for evaluation of Parkinson's disease. *Eur J Nucl Med Mol Imaging.* 2010;37:1594–1603.
28. Stoessl AJ, Martin WRW, McKeown MJ, Sossi V. Advances in imaging in Parkinson's disease. *Lancet Neurol.* 2011;10:987–1001.
29. Weng YH, Yen TC, Chen MC, et al. Sensitivity and specificity of ^{99m}Tc-TRODAT-1 SPECT imaging in differentiating patients with idiopathic Parkinson's disease from healthy subjects. *J Nucl Med.* 2004;45:393–401.
30. Wilson JM, Kish SJ. The vesicular monoamine transporter, in contrast to the dopamine transporter, is not altered by chronic cocaine self-administration in the rat. *J Neurosci.* 1996;16:3507–3510.
31. de la Fuente-Fernández R, Sossi V, McCormick S, Schulzer M, Ruth TJ, Stoessl AJ. Visualizing vesicular dopamine dynamics in Parkinson's disease. *Synapse.* 2009;63:713–716.
32. Sun J, Xu J, Cairns NJ, Perlmutter JS, Mach RH. Dopamine D1, D2, D3receptors, vesicular monoamine transporter type-2 (VMAT2) and dopamine transporter (DAT) densities in aged human brain. *PLoS ONE.* 2012;7:e49483.
33. Okamura N, Villemagne VL, Drago J, et al. In vivo measurement of vesicular monoamine transporter type 2 density in Parkinson disease with ^{18}F-AV-133. *J Nucl Med.* 2010;51:223–228.
34. Lu CS, Weng YH, Chen MC, et al. 99m Tc-TRODAT-1 imaging of multiple system atrophy. *J Nucl Med.* 2004;45:49–55.
35. Lin WY, Lin KJ, Weng YH, et al. Preliminary studies of differentia impairments of the dopaminergic system in subtypes of progressive supranuclear palsy. *Nucl Med Commun.* 2010;31:974–980.
36. Fearnley JM, Lees AJ. Ageing and Parkinson's disease: substantia nigra regional selectivity. *Brain.* 1991;114:2283–2301.
37. Kish SJ, Shannak K, Hornykiewicz O. Uneven pattern of dopamine loss in the striatum of patients with idiopathic Parkinson's disease. *N Engl J Med.* 1988;318:876–880.
38. Tolosa E, Gaig C, Santamaria J, Compta Y. Diagnosis and the premotor phase of Parkinson disease. *Neurology.* 2009;72:S12–S20.
39. Poletti M, Rosa AD, Bonuccelli U. Affective symptoms and cognitive functions in Parkinson's disease. *J Neurol Sci.* 2012;317:97–102.
40. Rahman S, Griffin HJ, Quinn NP, et al. Quality of life in Parkinson's disease: the relative importance of the symptoms. *Mov Disord.* 2008;23:1428–1434.
41. Ballanger B, Poisson A, Broussolle E, Thobois S. Functional imaging of non-motor signs in Parkinson's disease. *J Neurol Sci.* 2012;315:9–14.
42. Ito K, Nagano-Saito A, Kato T, et al. Striatal and extrastriatal dysfunction in Parkinson's disease with dementia: a 6-[^{18}F]fluoro-L-dopa PET study. *Brain.* 2002;125:1358–1365.
43. Remy P, Dorder M, Lees A, et al. Depression in Parkinson's disease: loss of dopamine and noradrenaline innervation in the limbic system. *Brain.* 2005;128:1314–1322.
44. Polito C, Berti V, Ramat S, et al. Interaction of caudate dopamine depletion and brain metabolic changes with cognitive dysfunction in early Parkinson's disease. *Neurobiol Aging.* 2012;33:206.e29–39.
45. Brooks DJ, Piccini P. Imaging in Parkinson's disease: the role of monoamines in behavior. *Biol Psychiatry.* 2006;59:908–918.